Health Indicators to Estimate Brake Rotor Thickness Variation

Hamed Kazemi[1], Xinyu Du[2], Samba Drame[3], Regan Dixon[4], and Hossein Sadjadi[5]

[1,3,4,5]*General Motors Canadian Technical Centre, Markham, Ontario, L3R 4H8, Canada*

hamed.kazemi@gm.com
samba.drame@gm.com
regan.dixon@gm.com
hossein.sadjadi@gm.com

[2]*General Motors Global Technical Centre, Warren, Michigan, 48092, USA*

xinyu.du@gm.com

ABSTRACT

Brake rotor thickness variation causes brake torque variation which can lead to brake judder and pulsation, steering wheel oscillations and chassis vibration. In this paper, we have proposed a prognostics methodology to predict the degradation level of brake rotor due to disc thickness variation. Leveraging the time and frequency domain analysis, this model creates health indicators to assess the health of the rotor and detect the rotor thickness variations of 36 micrometers or more. These health indicators that are calculated during braking events include: (i) envelope or variance of the brake master cylinder pressure (MCP); (ii) envelope or variance of the longitudinal acceleration (AX); (iii) the root mean square amplitude of the average order spectrum of the MCP at order one; and (iv) the root mean square amplitude of the average order spectrum of the AX at order one. This paper demonstrates that the above health indicators are significantly larger for a degraded brake rotor due to thickness variation compared to a healthy rotor.

1. INTRODUCTION

Brake rotors are critical components of the disc brake system. During braking, the brake hydraulic pressure squeezes a pair of pads against the rotor to generate friction. The pads retard the rotation of the shaft to reduce the rotational speed of the wheel. In this process, the kinetic energy is converted into heat, which is dissipated to the ambient environment.

Brake rotors can deteriorate in performance over their useful life and degrade for several reasons such as: (i) when brakes are applied intensely in quick succession; (ii) disc is worn below the minimum thickness; (iii) pads are excessively worn; and (iv) debris build between pads and disc. These factors normally reduce disc's capacity to dissipate heat and lead to thermal distortion and mechanical deflection (Antanaitis and Robere 2017).

Degraded rotors are the main source of "brake judder" where a non-uniform braking torque is applied to the vehicle resulting in brake force fluctuations (de Vries and Wagner 1992) & (Li, Meng and Zhang 2016). These fluctuations are perceived by driver as vibrations in steering wheel, pulsations in brake pedal, noise and vibrations from chassis components (Xu and Winner 2015). Brake judder can further be classified into thermal judder and cold judder. Thermal judder is due to uneven thermal expansion of the disc and occurs during deceleration from high speeds. Cold judder is the most common type of judder which is due to uneven wear or mounting and geometrical irregularities of the disc and occurs at any speed (Lee and Manzie 2016) & (Bryant, et al. 2008). The frequency of the judder is proportional to the wheel speed. Cold judder is mainly first and second order and causes lower frequency vibrations in the range of 10Hz to 100Hz, while hot judder causes higher frequency vibrations in the range of 10Hz to 600Hz (Xu and Winner 2015).

Common brake rotor failure modes include rotor thickness variation (RTV) – also known as DTV (Disc Thickness Variation), disc lateral runout, and corrosion. RTV refers to uneven surface of the brake rotor (Rodriguez 2006). RTV values greater than ~20 micrometers create noticeable brake judder for an experienced driver (de Vries and Wagner 1992).

Various chassis mechanical components, such as brake rotors, are not equipped with instrumentations to provide direct health monitoring and diagnostics. Therefore, when brake judder is felt by the driver, the thickness of the brake rotor is measured at multiple points to diagnose rotor faults. Significant research has been conducted in prognostics and health management (PHM) with numerous applications of rotary machinery components (bearings, gears, etc.) (Trilla,

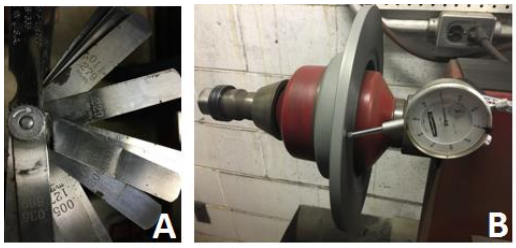

Figure 1. Generating first order thickness variation profile using feeler gauge (A) machining tool to create the variation (B).

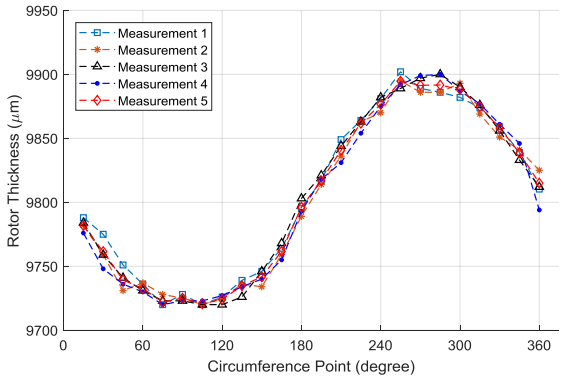

Figure 2. An example of rotor thickness measurements for case ID 5 with RTV of 180 µm. 180 was calculated as the median of the difference between maximum and minimum measured points (e.g. 180 µm = 9900 µm - 9720 µm)

Dersin and Cabre 2018), (Lee, et al. 2014), & (Butler, et al. 2012). Building on the existing PHM research, this paper demonstrates new prognostics capabilities to detect brake rotors thickness variation.

2. METHODS

This section provides information on procedures related to fault injection, measuring the degradation level (RTV), experimental setup, data acquisition, and the health indicators used to analyze rotor data and make predictions on the health of the brake rotor system.

2.1. Experimental Setup and Fault Injection

To create faulty rotors, parts of healthy rotors were machined down to generate varying levels of thickness variation. First order fault profile was injected which involves a uniform thickness variation using a feeler gauge as shown in Figure 1. When various rotor thickness measurements (about 24 points) were performed across various circumference points, a quasi-sinusoidal profile is produced, and the peak-to-peak amplitude of this profile is reported as RTV (see Figure 2). This procedure was repeated five times for each rotor and the median of the calculated RTVs were reported. In total, eight faulty rotors were created; Four faulty rotors were used in the front axle and four in the rear axle. Table 1 summarizes the various fault levels and fault locations.

Table 1. List of healthy and faulty brake rotors.

Case ID	Fault Level	Fault Location
1	5-10 µm	N/A
2	36 µm	Rear Left
3	126 µm	Rear Left
4	159 µm	Rear Left
5	180 µm	Rear Left
6	143 µm	Front Right
7	157 µm	Front Right
8	179 µm	Front Right
9	411 µm	Front Right

2.2. Measurement Setup and Signals

Numerous road tests were conducted, and data were collected using multiple GM production vehicles. In total, 1088 data sets were generated. 165 test cases were conducted with healthy rotors (i.e. RTV = 5-10 µm) and the remainder of the tests were performed with faulty rotors. The faulty rotor was installed in either front right corner or rear left corner. Data were collected under the following 12 noise factors:

- Velocity, deceleration rate, brake type, steering maneuver
- Vehicle mass, tire type, tire condition, tire pressure
- Road roughness, road friction, road bank angle, road grade

CAN signals were extracted in .mdf format with sampling frequency of 100 Hz using CANalyzer and were later exported to MATLAB 2017b for offline analysis. The main signals of interest included Master Cylinder Pressure (MCP), Longitudinal Acceleration (AX), Vehicle Speed (VS), Wheel Speed (WS), and Brake Pedal Position (BPP). It is important to note that the MCP, AX and WS are derived from three independent sensor sources.

2.3. Data Analysis

The AX and MCP signals were detrended using a moving average filter. Analyses were performed in both time domain and frequency domain to calculate signatures that are used to detect degradation. These signatures are called Health Indicators (HI) which can assess the health of the system and differentiate between a healthy and faulty rotor. Features were selected based on domain expert knowledge which suggested that the vibration analysis of the MCP, AX signals in time domain (variance) and frequency domain (average order spectrum) can be used to detect abnormalities (Du, et al. 2018). These signals were analyzed during brake events.

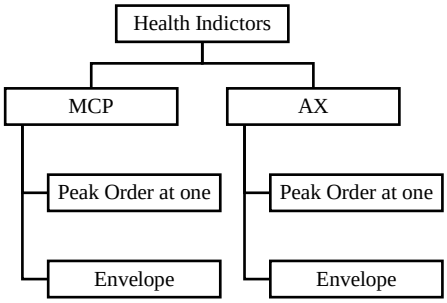

Figure 3. Health Indicators.

The brake event was identified using BPP and MCP signals and defined as when the BPP exceeds 0.5^0 above the resting position for a duration of at least one second and MCP exceeding one bar

2.4. Health Indicators

The following describes the health indicators that were calculated to differentiate between a healthy and faulty rotor and predict the failure level (RTV). Figure 3 shows the summary of the HIs used.

2.4.1. Envelope of the MCP and AX signal

The envelope of a signal is a smooth curve outlining the upper and lower bounds of the signal. The root-mean-square of the envelope of the MCP and AX during braking action was used as an HI to characterize the degradation level of the rotors. Figure 4 illustrates the envelope of the MCP signal during a breaking event.

2.4.2. Average Order Spectrum (AOS) of the MCP and AX signal

We analyzed the vibration of the MCP and AX signals using order analysis. Each order refers to a frequency that is a fixed multiple of a reference rotational speed. In this case, the first order refers to the number of events per each revolution of the wheel. The short-time Fourier transform of the MCP signal was computed and the RPM-frequency map was generated for a faulty rotor (case ID 9) which is shown in Figure 5-A. This waterfall plot indicates the frequency amplitudes that increase and decrease with the wheel speed RPM. By resampling the signal at constant phase increment and repeating the analysis using a short-time Fourier transformation, the spectral map of order as a function of RPM was generated and averaged over time to compute the Average Order Spectrum (AOS) depicted in Figure 5-B.

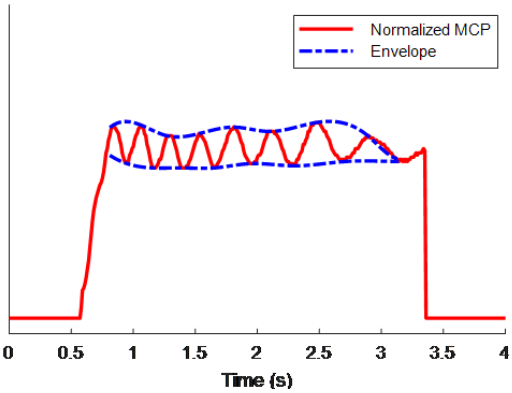

Figure 4. Envelope of the normalized MCP signal for a sample test case ID 4 demonstrating the envelope of the MCP signal with its upper and lower bound.

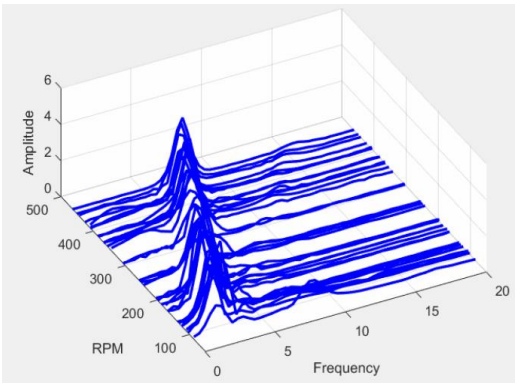

A

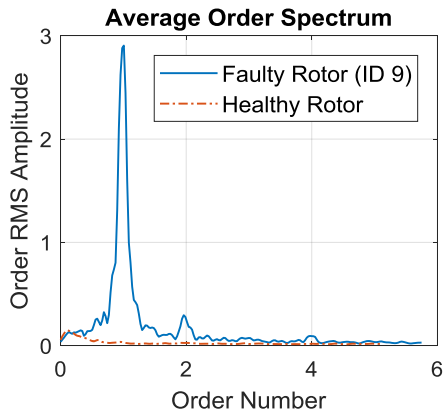

B

Figure 5. RPM-Frequency map of the MCP signal (A), average order spectrum of the MCP signal (B).

The average order spectrum indicates that there is a peak at first harmonic (order one). The RMS amplitude at order one is used as a feature or an HI to differentiate between a healthy and faulty rotor. The hypothesis put forward was that for faulty rotors the peak order at one is larger than healthy rotors. Similar analysis was performed on AX signal.

3. RESULTS AND DISCUSSION

Figure 6 shows a typical braking action illustrating MCP, AX, and WS signals for a healthy (case ID 1) rotor and a faulty rotor (case ID 8). In both examples, the vehicle speed decreased from about 60 Km/h to 20 km/h. The magnitude of

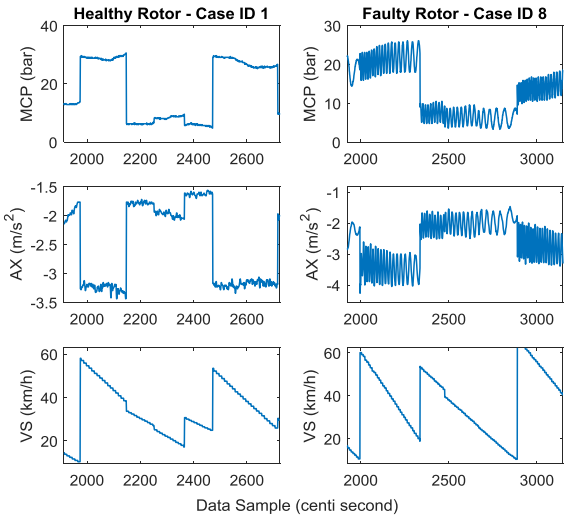

Figure 6. A representative data showing MCP, AX and VS signals during braking actions for a healthy (left) and a faulty (right) rotor

the MCP and AX were similar in both cases, but the visual inspection indicated that the variation in both MCP and AX signals were larger for the faulty rotor compared to the healthy one. This was a consistent behavior across all RTV levels. As RTV increased, the vibration and variance of both MCP and AX signals were also increased during braking actions.

3.1. Envelope of the MCP and AX Signal

Figure 7 shows a typical result from analysis of the envelope of the MCP signal for a healthy rotor and four different levels of RTV. BPP and MCP were normalized by their median and superimposed in each subplot. It can be seen that as RTV increases, the peak to peak of the envelope of the signal increases. This is further illustrated in Figure 8 where boxplot of the peak to peak envelope for MCP signal is plotted against the RTV. It also shows that for similar level of RTV, detecting a faulty rotor when it is located in the front wheel is easier than when it is in rear. The transfer of the load during deceleration to the front axle could play a role in observing larger vibration in front wheels.

3.2. Order Analysis of the MCP and AX Signal

Figure 5B shows the typical average order spectrum with a peak at first harmonic for MCP signal for a faulty rotor compared to a healthy rotor. A linear regression was performed to fit the MCP Peak Order HI to the response variable of rotor degradation level (i.e. measured RTVs). As an example, Figure 9A shows the histogram of the prediction of this linear regression model across all RTV levels for when the faulty rotor is installed in front right wheel. As can be seen there is a clear separation between the distribution of the faulty HIs versus healthy HI. Similar linear regressions were

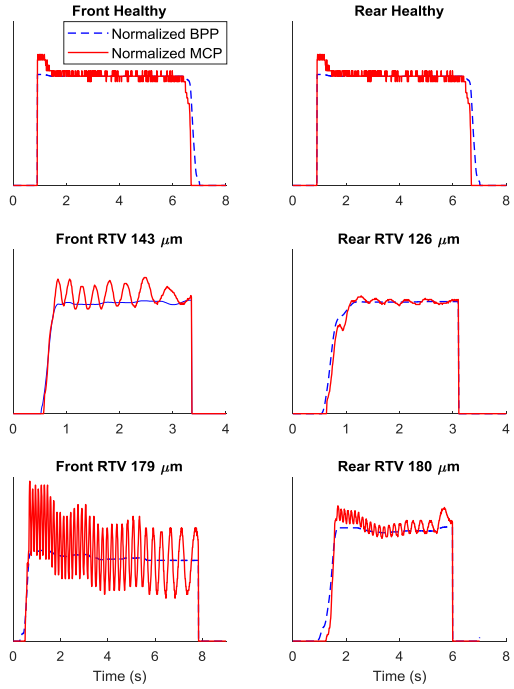

Figure 7. Normalized MCP and normalized BPP for healthy and faulty rotors with different RTVs.

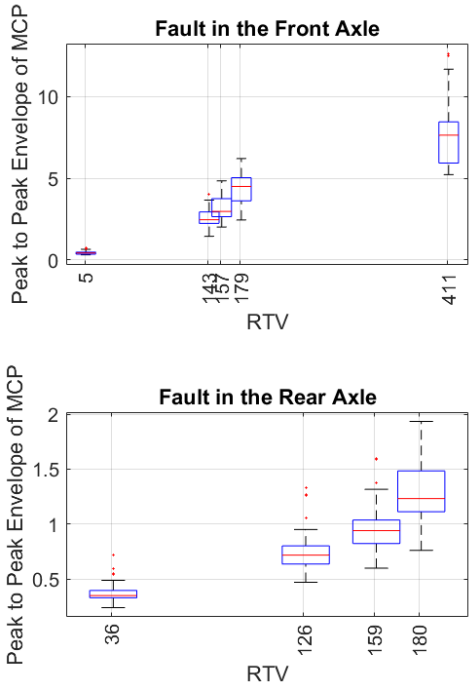

Figure 8. Peak to peak envelope of MCP signal as a function of RTV for healthy and faulty rotors.

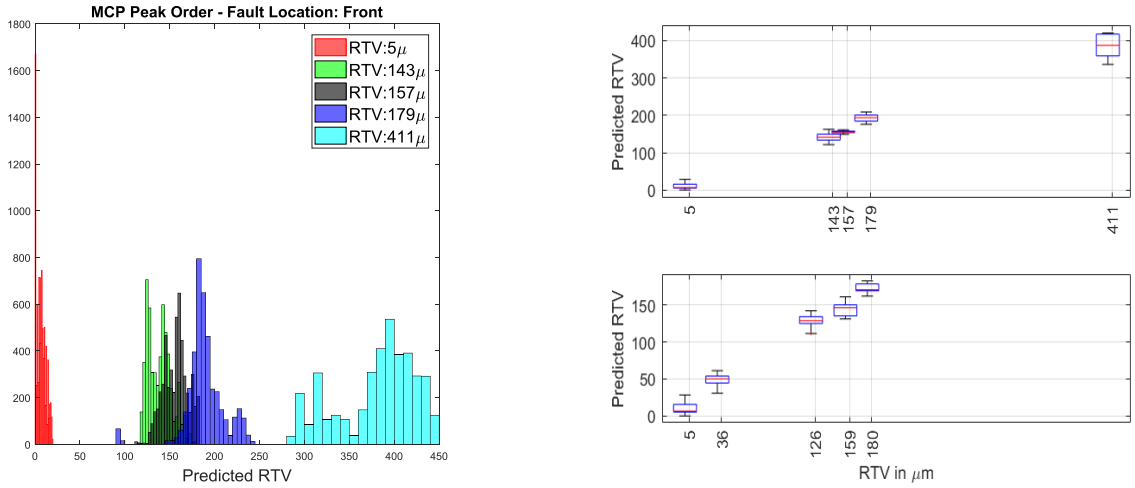

A B

Figure 9 Histogram of the RTV prediction of MCP Peak Order Health Indicator across all RTVs when the faulty rotor is in front wheel (A) and Boxplot of the predicted RTV using the Peak Order of the AX signal as an HI across all RTVs (B) for when the fault location is in front (Top) and is in rear (Bottom)

performed for other HIs. Figure 9B presents the boxplot of the prediction of the RTV peak orders for AX signals across all RTV levels. Even for the smallest RTV of 36, there is a clear separation between the distribution of the healthy rotor HI and the faulty rotor HI.

4. CONCLUSION

We investigated the effect of rotor thickness variation on characteristics of the braking action and derived a prognostics methodology to predict the failure levels of a faulty rotor degraded by thickness variations. Envelope and order analysis of the MCP and AX signals showed promising results in predicting the failure levels. Using each health indicator, we were able to successfully detect failure levels of 36 μm and larger.

ACKNOWLEDGEMENT

We thank Arash Mohtat, Graeme Garner, Qiugang Lu, Remi Guertin, Dongyi Zhou, Mutasim Salman, and Lichao Mai for their contribution to this project.

NOMENCLATURE

AX	Longitudinal Acceleration
MCP	Master Cylinder Pressure
BPP	Brake Pedal Position
AOS	Average Order Spectrum
VS	Vehicle Speed
WS	Wheel Speed
OA	Order Analysis
HI	Health Indicator
RTV	Rotor Thickness Variation

REFERENCES

Antanaitis, David B, and Matthew Robere. 2017. "Brake System Performance at Higher Mileage." SAE International Journal of Passenger Cars-Mechanical Systems 748-763.

Bryant, David, John D Fieldhouse, Andrew Crampton, Chris J Talbot, and Jonathan Layfield. 2008. "Thermal brake judder investigations using a high speed dynamometer." *SAE*.

Butler, Shane, Frank O'Connor, Des Farren, and John V Ringwood. 2012. "A feasibility study into prognostics for the main bearing of a wind turbine." *2012 IEEE International Conference on Control Applications* 1092-1097.

de Vries, Alexander, and Mark Wagner. 1992. "he brake judder phenomenon." *SAE Technical Paper*.

Du, Xinyu, Dongyi Zhou, Mutasim Salman, Kevin Cansiani, Xiaoyu Huang, and Wen-Chiao Lin. 2018. "detection of a friction brake fault". Patent filed.

Lee, Chih Feng, and Chris Manzie. 2016. "Active brake judder attenuation using an electromechanical brake-by-wire system." *IEEE/ASME transactions on mechatronics* 2964-2976.

Lee, Jay, Fangji Wu, Wenyu Zhao, Masoud Ghaffari, Linxia Liao, and David Siegel. 2014. "Prognostics and health management design for rotary machinery systems—Reviews, methodology and applications." *Mechanical systems and signal processing* 314-334.

Li, Mingzhuo, Dejian Meng, and Lijun Zhang. 2016. "Brake Judder Analysis Based on the Rigid-Flexible Coupling Model of Brake Corner." *SAE Technical Paper*.

Rodriguez, A. 2006. "Experimental analysis of disc thickness variation development in motor vehicle brakes." *Thesis.*

Trilla, Alexandre, Pierre Dersin, and Xavier Cabre. 2018. "Estimating the Uncertainty of Brake Pad Prognostics for High-speed Rail with a Neural Network Feature Ensemble." *PHM Society Conference.*

Xu, Xinfu, and Hermann Winner. 2015. "Experimental investigation of hot judder characteristics in passenger cars." *EuroBrake 2015* 1-12.